Journal of the Iranian Chemical Society (2021) 18:3377–3386
https://doi.org/10.1007/s13738-021-02273-1

ORIGINAL PAPER

Copper and chromium removal from synthetic textile wastewater using clay minerals and zeolite through the effect of pH

Sudipta Dasgupta[1] · Mohuli Das[1] · Marcos Antonio Klunk[2] · Soyane Juceli Siqueira Xavier[3] · Nattan Roberto Caetano[4] · Paulo Roberto Wander[2]

Received: 1 November 2020 / Accepted: 7 May 2021 / Published online: 22 May 2021

Abstract

The textile industries release a substantial amount of effluents into water resources every year. The vast majority of these effluents are composed of heavy metals that bind the textile fibres with dyes. This work proposes to use an adsorption system composed of clay-minerals (kaolinite and montmorillonite) and molecular sieve (zeolite) for separating the Cu^{2+} and Cr^{6+} ions, considering the pH changes of aqueous solutions. The adsorbent materials were characterized using the following state of the art techniques such as X-ray fluorescence, X-ray diffraction, Raman spectroscopy and Cation exchange capacity. During the adsorption tests, the contact time of the adsorbates (Cu^{2+} and Cr^{6+} ions in concentrations of 100, 50, 10 and 5 mg/L) with the adsorbents vary from 1 to 4 h in acidic and alkaline conditions (pH 3.5 and 7.5). The results indicate maximum adsorption of Cu^{2+} (at pH 3.5) and Cr^{6+} (at pH 7.5) ions on application of the zeolitic material. The clay minerals conclusively proved to be less efficient when compared to zeolite. It can be concluded that the adsorption system has achieved the desired efficiency, with substantial removal of Cu^{2+} and Cr^{6+} ions for zeolites in synthetic wastewater solutions of the textile industry.

Keywords Molecular sieves · Heavy metal · Adsorption process

Introduction

The disposal of heavy metals in the environment by the textile industry, tanneries and mining causes irreversible damage to the environment [1–4].These pollutants contribute to the increase in serious diseases, also causing an impact to their ambient environment and water resources [5, 6]. The pollution causing industries apply conventional processes to treat their effluents for the removal of Cu^{2+} and Cr^{6+} ions by chemical precipitation [7–9]. Decontamination of the water contaminated with traces of heavy metals by these processes is complicated. An efficient technique has been used in this study to predict the composition of wastewater, which is further used for chemical speciation modelling [10–12].

Some treatment technologies such as coagulation can also become a secondary source of contamination. The principal challenges of conventional treatments are the costs of final sludge disposal, the energy consumed and the necessary chemicals [13–15]. Therefore, the development of new clean technologies for water purification is crucial. The textile industries use several types of dyes. These compounds have two important components: (i) chromophore group (responsible for the colour) and (ii) functional group (has affinity with fibres of the fabric). Due to its applicability, there are hundreds of known dyes available in the industries. There are major differences between dyes and pigments that must be considered. Dyes are generally soluble or partially soluble in the substrate (textile materials, paper and leather). Therefore, the pigments are practically insoluble in the medium where they are applied [15–18]. Textile dyes are classified into: (i) basic or cationic (soluble in water); (ii) acids or anionic (soluble salts of sulfonic acid); (iii) direct ones, also called substrate dyes (fibres); (iv) mordants, which is bonded to the textile and cellulosic fibres employing an inorganic

✉ Marcos Antonio Klunk
marcosak@edu.unisinos.br

1 Indian Institute of Technology Bombay (IIT Bombay), Powai, Mumbai 400076, India

2 Department of Mechanical Engineering, University of Vale Do Rio Dos Sinos, Av. Unisinos 950, São Leopoldo, RS, Brazil

3 Department of Geology, University of Vale Do Rio Dos Sinos, Av. Unisinos 950, São Leopoldo, RS, Brazil

4 Federal University of Santa Maria, Av. Roraima 1000, Santa Maria, RS 97105-900, Brazil

agent (the most used is chromium in the form of oxide); (v) sulphur dyes (insoluble in water); (vi) non-ionic dispersions (insoluble in water) applied to synthetic fibres and (vii) reactive (form covalent bonds with cellulose and polyamide fibre substrates) [19–21].

Generally, dyes are not easily removable through traditional effluent treatment processes. Economically, removing colour remains a major problem for the industry. Due to the presence of heavy metals (such as chromium and copper), the separation systems are sometimes not efficient, dispersing these highly damaging elements to biota in the water resources [22–24]. Chromium removal from textile effluents is essential due to its toxicity. The speciations of chromium can be present in trivalent (Cr^{3+}) and/or hexavalent $(Cr_2O_7)^{2-}$ and $(CrO_4)^{2-}$ forms. The two forms of hexavalent chromium are dependent on pH of the medium, since in alkaline environments the chromate ion $(CrO_4)^{2-}$ predominates. Dichromate ions are more toxic than chromate ions [25, 26].

The removal of chromium from effluents can be achieved by various physico-chemical processes such as oxidation/reduction, precipitation/filtration, coagulation, ion exchange, and membrane separation [27]. These removal processes are hampered by the nature of the effluent (organic compounds, presence of other metals forming complexing agents) [28]. Another heavy metal found in textile effluents is copper. Like other metals, it accumulates in sediments and can be re-solubilized through the formation of complexes. Energy analysis of an effluent treatment system is important to identify the efficiency of the decontamination process. Thermodynamic losses which occur in a separation system are often not identified [29, 30]. It is highly toxic to fish, the toxicity increases in the presence of cadmium, zinc or mercury. One of the problems with copper removal is the presence of complex agents such as ammonia and cyanide, which form the stable complexes [31, 32]. Several adsorbents have been proposed to remove chromium and copper ions from aqueous solutions of textile effluents such as chitosan, activated carbon, biosorbents, and electrolytic processes. The disadvantage of these processes is the saturation of the adsorbent medium, as well as the energy expenditure associated with electrolytic precipitation [33]. An exergetic analysis is useful for identifying the causes and locations of the process inefficiencies. Despite the increased demand for more sustainable wastewater treatment systems, thermodynamic characterization is not fully developed [34, 35]. The adsorption process has the tendency to adhere the fluid phase molecules to the surface of a solid, due to attractive forces between the molecules. Adsorbent materials which have large surface area have a high adsorptive capacity [36, 37].

Depending on the strength of the bond with which the molecules are being adsorbed, the adsorption can be characterized by physics (the molecules or atoms adhere to the surface of the adsorbent, in general, through Van der Waals forces) or chemistry (the molecules or atoms adhere to the adsorbent surface through chemical bonds that are normally covalent) [38]. The primary factors affecting the adsorption capacity are: i) temperature (lower the temperature, greater is the amount adsorbed); ii) surface area (larger the surface area available for adsorption, greater is the amount of adsorbed metal) and iii) initial concentration of adsorbate (increase in the concentration of adsorbate can accelerate the diffusion of solution molecules into solid surface) [39–41].

This work aims to recreate various concentrations of Copper (Cu^{2+}) and Chrome (Cr^{6+}) (100, 50, 10, and 5 mg/L) in a textile effluent with two clay minerals (kaolinite and montmorillonite) and a molecular sieve (zeolite). The concentration of the ions was analysed by ICP-OES (inductively coupled plasma optical emission spectrometry) and was measured in triplicates. XRF (X-ray fluorescence), XRD (X-ray diffraction), Raman spectroscopy and cation exchange capacity (CEC) were used to characterize the adsorbents. The contact time of the adsorbent in the adsorbate was 1, 2, 3, and 4 h with a pH varying from 3.5 to 7.5. Here, the adsorption system used is according to the studies by Klunk et al. [42]. The results indicated that at acidic pH, there was a greater efficiency of removal of Cr^{6+} using zeolite. And for alkaline pH, there was greater efficiency in removing Cu^{2+} with zeolites. The utility of low-cost adsorbents has been considered to be a great alternative for the removal of copper and chromium reaching concentrations below the detection limit.

Materials and methods

Clays mineral and molecular sieves play an important role in the environment, effectively removing toxic metal ions from aqueous solution. The use of these materials as adsorbents has advantages in terms of low cost, availability, high specific surface area, non-toxic nature and great potential for ion exchange. To attain the objectives of the present study, kaolinite, montmorillonite and zeolite were used with reference to Klunk et al. [43]. Kaolinite has been extensively used to remove heavy metal ions, despite its low cation exchange capacity. Its structure belongs to type 1:1 with a tetrahedral layer of silica (SiO_2) joined to an oxygen atom and an octahedral layer of alumina (Al_2O_3). Kaolinite has high chemical stability and low capacity for expansion and cation exchange [44, 45]. Montmorillonite has a 2:1 structure with an octahedral alumina layer sandwiched between two opposite layers of tetrahedral silica. The bond between two layers of silica is very weak, allowing water and exchangeable ions to enter. This leads to a high ion exchange capacity [46]. Molecular sieves are composed of well-defined crystalline structures. They consist of crystalline aluminosilicates with a three-dimensional

structure of silicon and aluminium tetrahedron [47]. The combination of these structures creates minerals with interstitial cavities. These structures cause the zeolites to have an extremely large internal surface compared to the external surface. Zeolitic materials are differentiated by the Si/Al (SAR) ratio. A zeolite's cation exchange capacity is related to its SAR [48]. The ability to exchange cations inside the zeolite cavities gives it the characteristics of an efficient material in adsorption.

Adsorption systems

The adsorption study of Cu^{2+} and Cr^{6+} ions in clay minerals and molecular sieve were investigated in four different concentrations (100, 50, 10 and 5 mg/L) for a period of 1 to 4 h at pH 3.5 and 7.5. The aqueous solution containing the ions (Cu^{2+} and Cr^{6+}) recreated a textile effluent with a load of toxic heavy metals. The operational procedure of the adsorption system considers that the samples are completely covered with the adsorbent and kept under agitation for 30 min [49]. Post this procedure, the samples were transferred to the adsorptive system (glass column) according to the studies by Klunk et al. [42]. The ion removal efficiency was estimated using the following equation:

$$\%\ \text{ions removal} = \left[\left(C_i - C_f\right)/C_i\right] \times 100$$

where C_i and C_f are the initial and final concentration at time t (mg/L) of ions in the solution. The initial and final concentration were analysed by ICP-OES and measured in triplicates. For each adsorptive medium, a fixed amount of 5 g of kaolinite, montmorillonite and zeolite with 20 mL aliquots of the ions Cu^{2+} and Cr^{6+} at different time intervals (1, 2, 3 and 4 h) were used. The synthesis of zeolite has been developed based on the research work of Klunk et al. [50]. Highly pure kaolinite and montmorillonite (Sigma Aldrich) were used for the experiment.

Characterization of materials

To understand the adsorption process, adsorptive materials need to be characterized by techniques that can reveal their peculiarities. Therefore, the characteristics analysed (with analytical techniques) in this particular study are: (i) specific surface area (BET), (ii) chemical composition (XRF), (iii) mineral composition (XRD), (iv) chemical structure and molecular interactions (RAMAN) and (v) cation exchange capacity (CEC) [51–55].

Results and discussion

Characterization of clay minerals and molecular sieve

Below are the results documenting the characterization of constituent materials present in the adsorption system. Table 1 shows the values of the textural properties of these adsorbents. The clay minerals (kaolinite and montmorillonite) presented a specific surface area in the order of 34.82 and 39.66 m^2/g, respectively. The pore volume of these materials varies from 0.322 cm^3/g (kaolinite) to 0.393 cm^3/g (montmorillonite). In addition, the average pore diameter of montmorillonite is 17% higher than kaolinite. When these comparisons occur with zeolite, the scenario changes. Zeolite has 51% more specific surface area (59.87 m^2/g) than montmorillonite. The comparison of pore volume of zeolite with montmorillonite shows an increase of 22%.

The average pore diameter of montmorillonite is 20% less than zeolite. Figure 1 demonstrates the N_2 adsorption/desorption isotherms for the adsorbent samples. It can be observed in the adsorption materials' isotherms that an increase in the relative pressure (p/p_0) occurs in the range of 0.01 and 0.98. For montmorillonite (Fig. 1A) the relative pressure (p/p_0) varies between 0.35 and 0.98 where a rapid absorption occurs, thereby indicating the existence of empty cavities in the crystalline structure of the clay mineral. Additionally, this relative pressure (p/p_0) indicates mesoporous channels. For kaolinite (Fig. 1B) and zeolite (Fig. 1C) the relative pressures (p/p_0) fluctuate between 0.82 to 0.98 and 0.65 to 0.98, respectively. Such behaviour can be interpreted by the fact that kaolinite and zeolite are filling the pores of their crystalline structure, which means the presence of mesoporous cavities.

The obtained isotherms demonstrated that all samples exhibit the typical type IV adsorption isotherm with H3 hysteresis loop as identified by IUPAC [56, 57]. The characteristics of the three raw materials are displayed in Table 2. The potential applications as kaolinite, montmorillonite and zeolite adsorbents were defined by the chemical composition determined by X-ray fluorescence. The results are based on the most stable forms of inorganic

Table 1 Textural properties for clay minerals and zeolite

Adsorbent	BET surface area (m^2/g)	Pore volume (cm^3/g)	Average pore diameter (nm)
Kaolinite	34.82	0.322	3.45
Montmorillonite	39.66	0.393	4.03
Zeolite	59.87	0.485	4.82

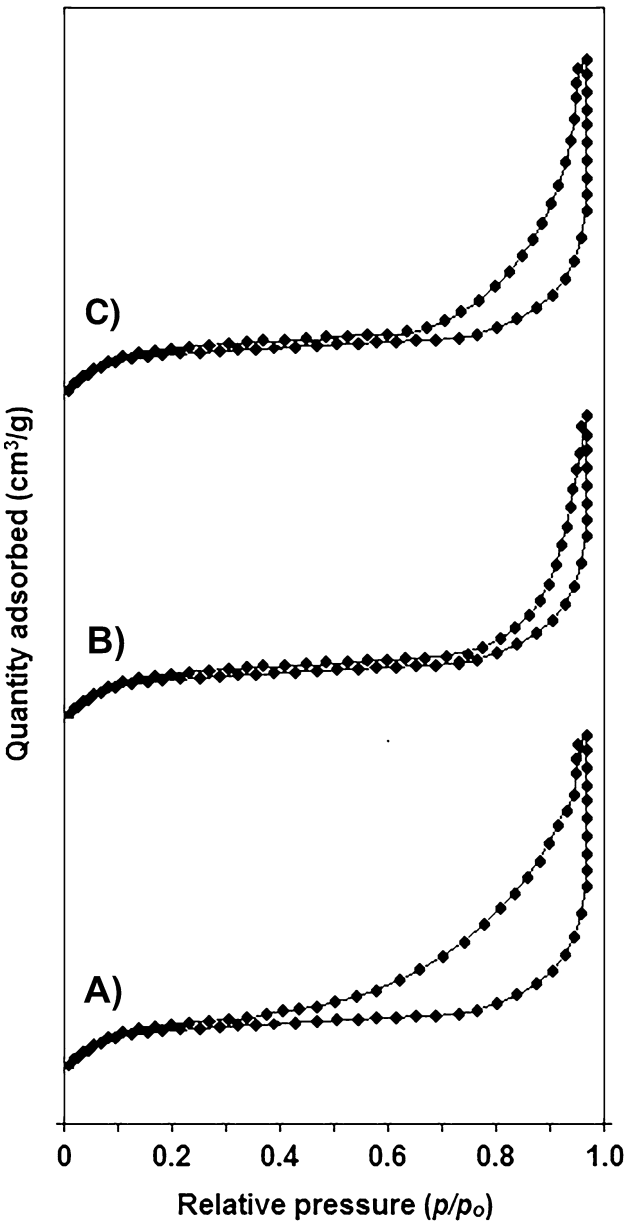

Fig. 1 N_2 adsorption and desorption isotherms of montmorillonite (A), kaolinite (B) and zeolite (C)

oxides detected by the equipment. The results indicate a significant variation among the primary components of clay minerals and zeolite.

For kaolinite, X-ray fluorescence reveals a high amount of alumina (39.02) when compared to other materials. High quantity of Al_2O_3 in the kaolinite crystalline lattice favours the high structural stability of alumina octahedrons (Al_2O_3), causing low exchange capacity among other elements. This behaviour is evidenced by the low SiO_2/Al_2O_3 (1.15) ratio responsible for the permutation phenomenon.

Montmorillonite and zeolite, in general, revealed high silica content with low quantity of alumina and ferric oxide.

Table 2 Chemical analysis obtained by X-Ray Fluorescence Spectroscopy for kaolinite, montmorillonite and zeolite (% by mass)

Oxides	Kaolinite	Montmorillonite	Zeolite
SiO_2	44.93	51.37	59.48
Al_2O_3	39.02	18.20	17.71
Fe_2O_3	3.89	1.10	0.94
Na_2O	0.41	3.38	2.73
K_2O	1.72	4.22	1.17
CaO	2.89	1.15	2.41
MgO	0.50	4.43	0.81
TiO_2	0.51	0.95	1.02
SO_3	0.23	0.39	0.33
SiO_2/Al_2O_3	1.15	2.82	3.36

For this reason, the SiO_2/Al_2O_3 ratios of montmorillonite (2.82) and zeolite (3.36) favour cation exchange and consequently, greater adsorption capacity in their structures.

To identify the formation of crystalline structures and the mineral composition of the adsorbent materials, the X-ray diffraction technique is the most suitable and successful. The diffractograms obtained are documented in Fig. 2. In the clay mineral samples and molecular sieve, bands were obtained corresponding to the crystalline phases of the studied materials.

The results were identified based on the International Union Database Crystallography's Joint Committee on Powder Diffraction Standards (JCPDS) [52, 53]. The relative crystallinity was calculated according to the aggregated intensities of the characteristic diffraction peaks for each adsorbent. The chemical formulas of the crystalline phases of the minerals present in the adsorbents are shown in Table 3. In Fig. 2A the diffractogram corresponding to montmorillonite (2θ of 6.5°, 12.8° and 58.1°) has been documented. The existence of crystalline phases such as muscovite (2θ of 9.8° and 38.2°), kaolinite (2θ of 12.5° and 17.9°), quartz (2θ of 19.9°, 21.8°, 40°, 45° and 50°), feldspar (2θ of 21.8°), illite (2θ of 35.1°) and mica (2θ of 61.8°) have also been observed.

On the other hand, the kaolinite diffractogram (2θ of 12.5°, 17.9°, 20.1°, 23.2°, 25.0°, 35.1°, 36.2°, 38.0°, 39.3°, 45.5°, 48.4°, 56.2° and 62.5°) is displayed in Fig. 2B. Crystalline phases appear as quartz (2θ of 19.8° and 30.2°) and dickite (2θ of 26.0°). Finally, in Fig. 2C the diffractogram of the zeolitic material corresponding to sodalite (2θ of 14.2°, 20.1°, 25.2° and 43.9°) has been shown. In this zeolite, the presence of mullite (2θ of 31.5°), kaolinite (2θ of 35.1°, 38.0°, 45.5°, 48.4° and 51.2°) and quartz (2θ of 53.5°, 54.0°, 59.1°, 61.2°, 63.4° and 64.8°) has been studied. The presence of sodalite is reinforced by X-ray fluorescence (Table 2), which shows the characteristic SiO_2/Al_2O_3 3.36 ratio for sodalite.

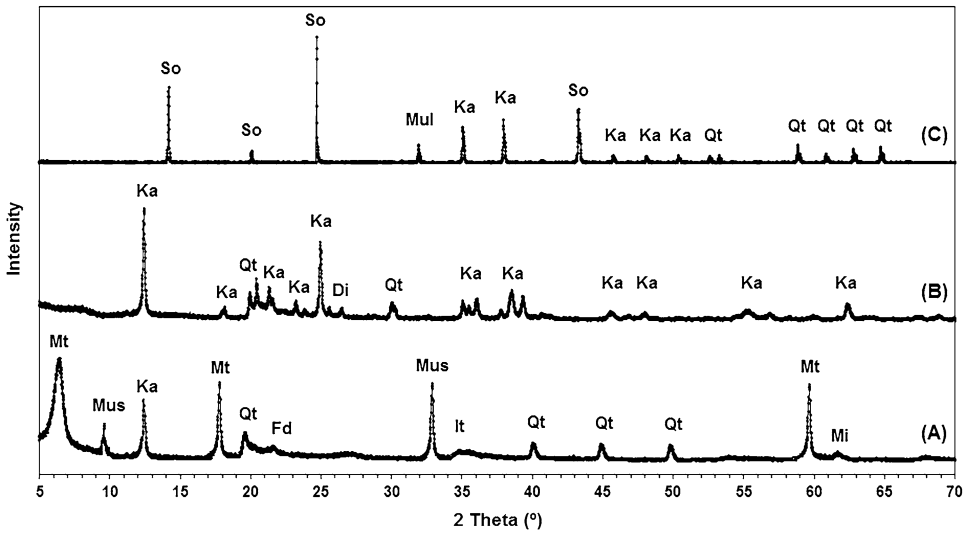

Fig. 2 Diffractogram of (A) montomorillonite, (B) kaolinite and (C) zeolite. The crystalline phase is Mt: Montmorillonite; Mus: Muscovite; Ka: Kaolinite; Qt: Quartz; Fd: Feldspar; It: Illite; Mi: Mica; Di: Dickite; So: Sodalite; Mul: Mullite

Table 3 Crystalline structures and chemical formula of the compounds presents in materials

Crystalline structures	Chemical formula
Montmorillonite	$MgNaAl_5(Si_4O_{10})_3(OH)_6$
Kaolinite	$Al_2Si_2O_5(OH)_4$
Sodalite	$Na_8Al_6Si_6O_{24}Cl_2$
Mullite	$Al_{4,44}Si_{1,56}O_{9,78}$
Quartz	SiO_2
Muscovite	$KAl_2(AlSi_3O_{10})(OH)_2$
Feldspar	$KAlSi_3O_8$
Illite	$KAl_2(Al_4Si_4O_{10})(OH)_2$
Mica	$KAl_2(AlSi_3O_{10})(OH)_2$
Dickite	$Al_2Si_2O_5(OH)_4$

Raman spectroscopy is a technique used to identify minerals. The spectra of Raman function as a mineral signature [54]. The results of Raman spectroscopy are displayed in Fig. 3A–C. In montmorillonite (Fig. 3A), high intensity bands of 80 and 1200 cm^{-1} refer to the vibration of interlayer cations and Si–O, respectively. Moderate intensity bands identified the bonds of the clay mineral tetrahedra with O–Al–O (250 cm^{-1}), Si–O–Si (558 cm^{-1}), Al–OH (749 cm^{-1}) and Mg–Al–OH (850 cm^{-1}).

Therefore, for kaolinite (Fig. 3B), low intensity bands referring to the O–Si–O (122 cm^{-1}), Si–O (1240 cm^{-1}) and hydroxyl (1600 cm^{-1}) have been identified. For high intensity bands, the kaolinite spectrum reveals the presence of the O–Al–O (230 cm^{-1}), Si–O (410 cm^{-1}), Si–O–Si (560 cm^{-1}) and Al–OH (680 cm^{-1}). Finally, Raman spectroscopy identified the structural bonds of low and high intensity for the zeolitic material (Fig. 3C). In this way, the Cl–Na (74 cm^{-1}), Na–O (160 cm^{-1}) and O–Al–O (285 cm^{-1}) connections have been identified, referring to the formation of Sodalite zeolite. This molecular sieve is proven by identification of chemical formula and crystalline structures with the aid of XRF (Table 2) and XRD (Table 3), respectively. The Sodalite structure has the vibrations of Al–Si (360 cm^{-1}) and Si–O (680 cm^{-1}).

Raman spectroscopy is a powerful tool to complement other characterization techniques. In this regard, the vibrations of the bonds between clay-minerals and zeolitic material reveal the characteristic structures of the adsorbent materials [58]. The cation exchange capacities (CEC) were determined by the inductively coupled plasma optical emission spectrometry (ICP-OES). The values of the cation exchange capacity of the adsorbent materials are demonstrated in Table 4. The CEC results for clay minerals are 50% higher for montmorillonite. This was due to the greater specific surface area (Table 1) of montmorillonite when compared to kaolinite.

When these results are compared to the zeolitic material, it is evident that the molecular sieve performs the cationic exchanges more efficiently, leading to 3.61 fold greater than the best quality clay mineral. Zeolite has 1.51 times greater specific surface area when compared to montmorillonite. The high CEC values of the zeolitic material are related to the availability of SiO_2 and Al_2O_3 in the crystalline lattice which allow the exchange of ions in the mineral's tetrahedrons. The results of XRD (Fig. 2) that revealed the diffractograms profiles of the various crystalline materials present in the samples are the proof for that. The CEC values found for sodalite zeolite reveals that these materials have high potential as ion exchangers. The adsorption process of Cu^{2+} and Cr^{6+} ions were investigated in four different concentrations (100, 50, 10, and 5 mg/L), two pH variations (3.5 and 7.5), and adsorption time of the aqueous solutions in the adsorptive system

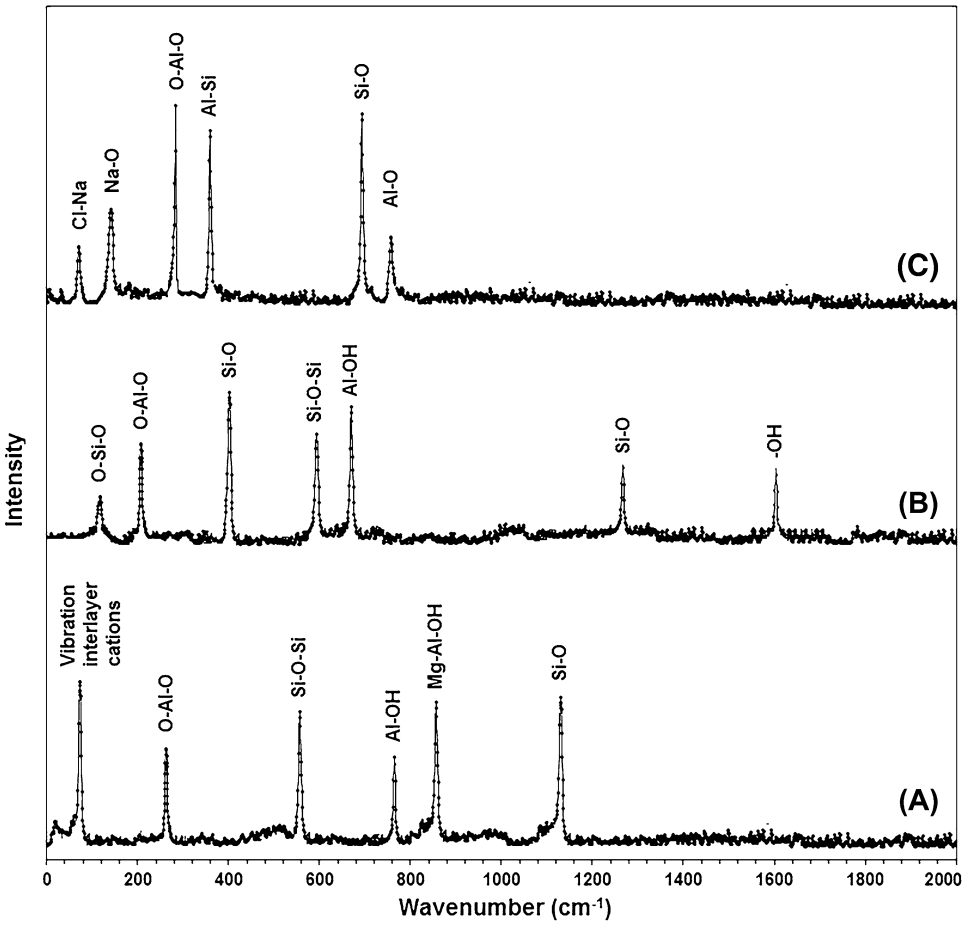

Fig. 3 Raman spectroscopic of (A) montmorillonite, (B) kaolinite and (C) zeolite

Table 4 CEC values for clay minerals and zeolite

Si/Al Ratio	CEC (meq/g)	Average
Montmorillonite	0.82	0.80
	0.80	
	0.79	
Kaolinite	0.56	0.54
	0.54	
	0.53	
Zeolite	2.92	2.90
	2.89	
	2.88	

from 1 to 4 h. The results (removal % of the ions) are exhibited in Fig. 4 (Cu^{2+} ions) and Fig. 5 (Cr^{6+} ions).

Figure 4 shows the greatest efficiency in the removal of Cu^{2+} ions occurs at alkaline pH. The adsorbent material having the greatest retention power for copper ions is zeolite. The pH 7.5 promotes the mobility of Cu^{2+} ions making it easier for zeolite to promote ion exchange in the crystalline lattice. This kind of pH behaviour can be explained by variations in the surface charge of alumina during the adsorption process. At alkaline pH, alumina is responsible for cationic exchange between the crystalline structure of zeolite and Cu^{2+} ions present in the solution. In this way, an exchange occurs between the copper ions (entering the zeolite cavity) and Al^{3+} ions (that exit the structure). When Al^{3+} ions exit the zeolitic structure, they combine the hydroxyl (–OH) compounds, giving an alkaline character to the solution.

In Fig. 5, the influence of acidic pH can be found during the removal of Cr^{6+} ions in aqueous solution. The alkaline pH favours the removal of Cu^{2+}, at pH 7.5. The efficiency of the adsorption process is more successful for Cr^{6+} ions. The adsorbent material showing the best performance in the adsorptive process was zeolite. This tendency can be explained by the exchange of cations in the zeolitic structure, releasing H^+ by Cr^{6+} ions. At the beginning of the adsorption process, ion exchange with the H^+ ions takes place in the solution, where the substituted Cr^{6+} ions occupy the sites vacated by the H^+ ions. Consequently, it has been studied that higher concentration of H^+ ion in solution results in lower pH of the solution after adsorption.

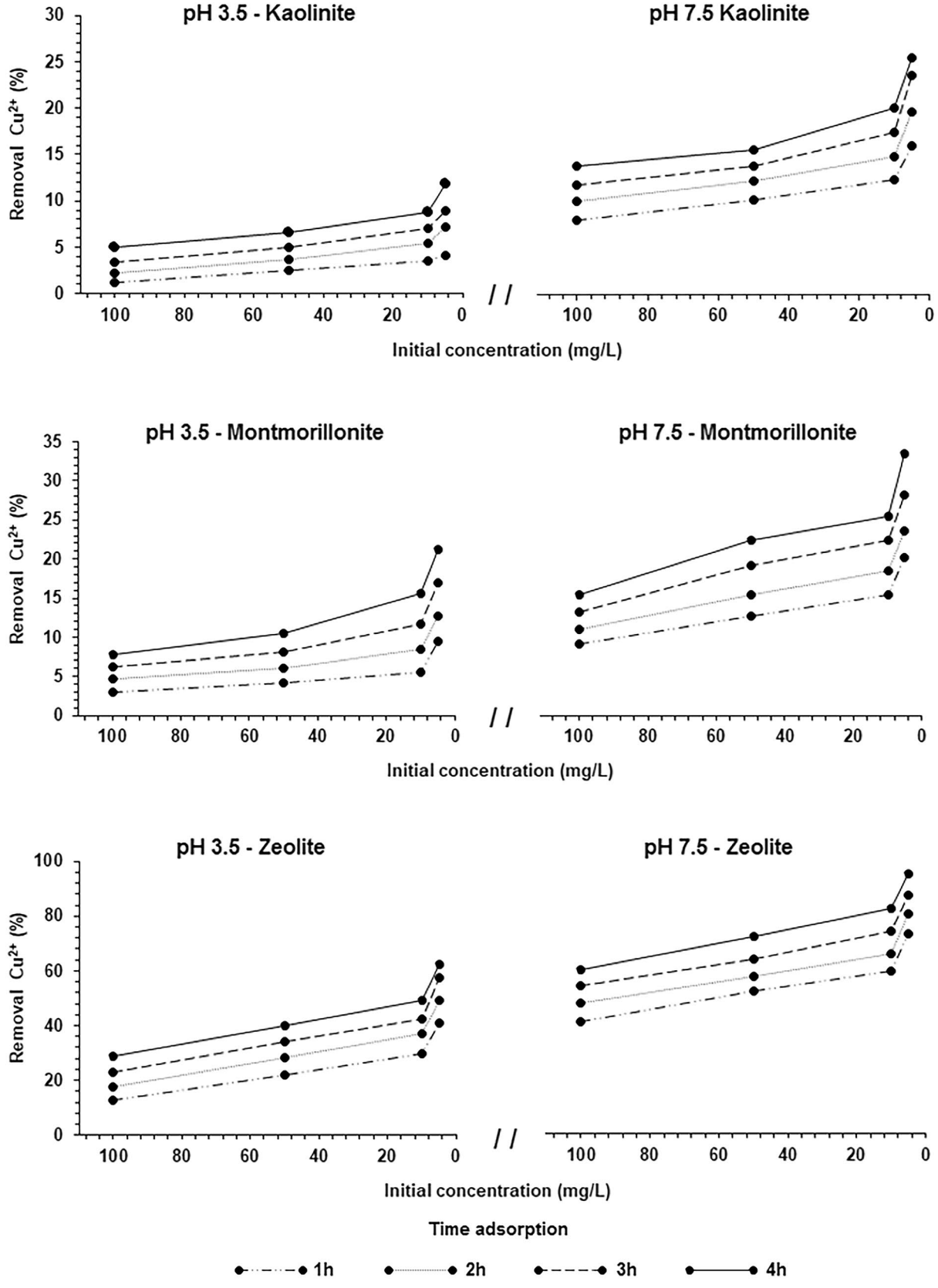

Fig. 4 Percentage of removal Cu^{2+} in adsorbent materials

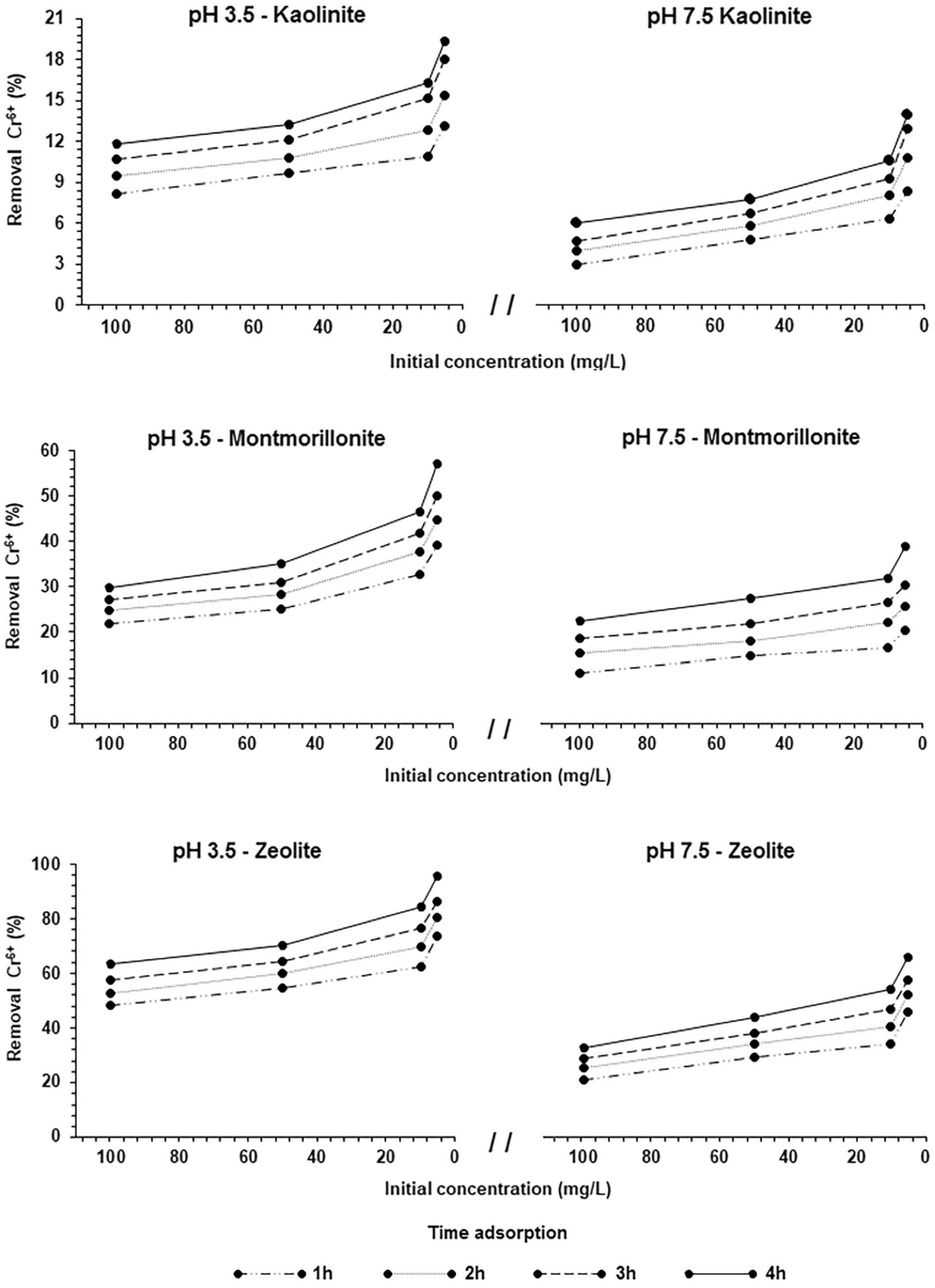

Fig. 5 Percentage of removal Cr^{6+} in adsorbent materials

Conclusions

In the present work, clay minerals and molecular sieve have been used as adsorbents for adsorption of Cu^{2+} and Cr^{6+} ions in aqueous solution. These ions were selected to simulate a textile effluent due to the presence of toxic heavy metals. The characterization of the adsorbent materials was fundamental to understand the adsorption process.

The average pore diameter of montmorillonite is 17% greater than kaolinite and 20% less than zeolite. Zeolite has 51% more specific surface area and 22% more pore volume than montmorillonite. The N_2 adsorption/desorption isotherms demonstrated that all samples exhibit the typical type IV adsorption profile with H3 hysteresis loop, which is the characteristic of the material having porous cavities in the structure. Montmorillonite and zeolite, in general, displayed high silica content with low amounts of alumina and ferric oxide, favouring cation exchange and consequently greater adsorption capacity.

X-ray diffraction reveals the crystalline structures and chemical formula of the compounds present in adsorbent materials. This technique aided in the acquisition of high crystallinity of the samples, corresponding to high purity of the materials. As a complementary technique, Raman spectroscopic analysis identified mineral signatures of montmorillonite, kaolinite and zeolite with intense bands, among other compounds. CEC revealed that zeolite is an easier medium to exchange ions than clay minerals, being 3.61 fold more efficient.

The adsorption process of the Cu^{2+} and Cr^{6+} ions has a direct influence on the pH of the medium. The results allow concluding that for alkaline pH there was greater adsorption of Cu^{2+} and for acid pH, the adsorption of Cr^{6+} ions was more successful. Both results obtained by the adsorption process were more efficient using zeolite. The clay minerals had decent adsorption capability, but is less effective when compared to the molecular sieve. Henceforth, it can be concluded from the present study that the adsorption system has potential for effective removal of Cu^{2+} and Cr^{6+} ions from wastewater of the textile industry.

Acknowledgements The authors acknowledge the Brazilian agencies of CNPq (National Council of Technological and Scientific Development – Brasília, DF, Brazil), CAPES (Coordination for the Improvement of Higher Education Personnel) and the Indian agencies such as IRCC (Industrial Research and Consultancy Centre), Indian Institute of Technology Bombay, MoE (Ministry of Education), India for the research funding and research grants of the Brazilian (PNPD/CAPES and DT2/CNPq) and Indian authors, respectively. The authors also acknowledge generous cooperation and assistance of all the people from the company who granted us access to their database and perception.

Funding This research did not receive financial assistance.

Declarations

Conflict of interest The authors declare that they have no conflict of interest.

References

1. L. Hossain, S.K. Sarker, M.S. Khan, Environ. Dev. **26**, 23–33 (2018). https://doi.org/10.1016/j.envdev.2018.03.005
2. Z. Hussain, M. Arslan, M.H. Malik, S. Iqbal, M. Afzal, Sci. Total Environ. **645**, 966–973 (2018). https://doi.org/10.1016/j.scitotenv.2018.07.163
3. E. Hassanzadeh, M. Farhadian, A. Razmjou, N. Askari, Environ. Nanotechnol. Monit. Manage **8**, 92–96 (2017). https://doi.org/10.1016/j.enmm.2017.06.001
4. A. Taavoni-Gilan, E. Taheri-Nassaj, M. Shamsipur, J. Iran. Chem. Soc. **15**, 2759–2769 (2018). https://doi.org/10.1007/s13738-018-1463-3
5. K. Nadeem, G.T. Guyer, B. Keskinler, N. Dizge, J. Clean Prod. **228**, 1437–1445 (2019). https://doi.org/10.1016/j.jclepro.2019.04.205
6. M.A. Klunk, A. Oliveira, G. Furtado, G.H. Knornschild, L.F.P. Dick, ECS Trans. **43**, 23–27 (2012). https://doi.org/10.1149/1.4704934
7. R. Ansari, Z. Mosayebzadeh, Chem. Pap. **65**, 1–8 (2011). https://doi.org/10.2478/s11696-010-0083-x
8. M. Szynkowska, E. Rybicki, E. Leśniewska, A. Pawlaczyk, T. Paryjczak, E. Matyjas-Zgondek, Chem. Pap. **63**, 537–542 (2009). https://doi.org/10.2478/s11696-009-0044-4
9. L.D.O. Pereira, R.V. Lelo, G.C.M. Coelho, F. Magalhães, J. Iran. Chem. Soc. **16**, 2281–2289 (2019). https://doi.org/10.1007/s13738-019-01694-3
10. M.A. Klunk, L.H. Damiani, G. Feller, M.F. Rey, R.V. Conceiçao, M. Abel, L.F. De Ros, Braz. J. Geol. **45**, 29–45 (2015). https://doi.org/10.1590/2317-4889201530145
11. M.A. Klunk, S. Dasgupta, R.V. Conceiçao, J. Palaeogeogr. **7**, 12–26 (2018). https://doi.org/10.1186/s42501-018-0009-z
12. M.A. Klunk, S. Dasgupta, S.B. Schropfer, B.V.G. Nunes, P.R. Wander, Per. Tchê Quím. **16**(31), 816–822 (2019)
13. P.R. Wander, F.M. Bianchi, N.R. Caetano, M.A. Klunk, M.L.S. Indrusiak, Energy **203**, 117882 (2020). https://doi.org/10.1016/j.energy.2020.117882
14. R. Cataluña, Z. Shah, V. Venturi, N.R. Caetano, B.P. Da Silva, C.M.N. Azevedo, R. Da Silva, P.A.Z. Suarez, L.P. Oliveira, Fuel **228**, 226–233 (2018). https://doi.org/10.1016/j.fuel.2018.04.167
15. R. Cataluña, Z. Shah, L. Pelisson, N.R. Caetano, R. Da Silva, C. Azevedo, J. Braz. Chem. Soc. (2017). https://doi.org/10.21577/0103-5053.20170100
16. A. Fraga, M.A. Klunk, A. Oliveira, G. Furtado, G.H. Knornschild, L.F.P. Dick, Mater. Res. **17**, 1637–1643 (2014). https://doi.org/10.1590/1516-1439.305714
17. T. Madrakian, A. Afkhami, N. Rezvani-jalal, M. Ahmadi, J. Iran. Chem. Soc. **11**, 489–498 (2014). https://doi.org/10.1007/s13738-013-0322-5
18. Y. Sürme, O. Demirci, Chem. Pap. **68**(11), 1491–1497 (2014). https://doi.org/10.2478/s11696-014-0616-9
19. M. Šimek, P. Mikulášek, P. Kalenda, T. Weidlich, Chem. Pap. **70**(4), 470–476 (2016). https://doi.org/10.1515/chempap-2015-0225
20. N. Bahadur, N. Bhargava, J. Water Process. Eng. **32**, 100934 (2019). https://doi.org/10.1016/j.jwpe.2019.100934
21. L. Zhou, K. Xu, X. Cheng, Y. Xu, Q. Jia, J. Clean. Prod. **141**, 721–727 (2017). https://doi.org/10.1016/j.jclepro.2016.09.047

22. A.C. Ruoso, L.C. Bittencourt, L.U. Sudati, M.A. Klunk, N.R. Caetano, Per. Tchê Quím **16**(32), 560–571 (2019)
23. S.M. Stagnaro, M.C. Volzone, L. Huck, Proc. Mater. Sci. **8**, 586–591 (2015). https://doi.org/10.1016/j.mspro.2015.04.112
24. S. Rangabhashiyam, N. Anu, N. Selvaraju, J. Environ. Chem. Eng. **1**(4), 629–641 (2013). https://doi.org/10.1016/j.jece.2013.07.014
25. A.C. Ruoso, A. Lhamby, A.B. Missaggia, M.A. Klunk, N.R. Caetano, Per Tchê Quím. **17**(34), 220–239 (2020)
26. M.A. Klunk, S. Dasgupta, M. Das, P.R. Wander, Per. Tchê Quím. **16**(32), 108–118 (2019)
27. M.A. Klunk, S. Dasgupta, M. Das, P.R. Wander, A. Di Capua, Per. Tchê Quím. **16**(33), 736–748 (2019)
28. A.M. Ferreira, J.A.P. Coutinho, A.M. Fernandes, M.G. Freire, Sep. Purif. Technol. **128**, 58–66 (2014). https://doi.org/10.1016/j.seppur.2014.02.036
29. R.M. Jain, K.H. Mody, J. Keshri, B. Jha, Mar. Pollut. Bull. **84**(1–2), 83–89 (2014). https://doi.org/10.1016/j.marpolbul.2014.05.033
30. U. Lucia, G. Grisolia, Energy Rep. **5**, 62–69 (2019). https://doi.org/10.1016/j.egyr.2018.12.001
31. U. Lucia, M. Simonetti, G. Chiesa, G. Grisolia, Renew. Sustain. Energ. Rev. **70**, 867–874 (2017). https://doi.org/10.1016/j.rser.2016.11.268
32. S. Islam, G. Bhat, J. Environ. Manage. **251**, 109536 (2019). https://doi.org/10.1016/j.jenvman.2019.109536
33. M.A. Klunk, Z. Shah, N.R. Caetano, R.V. Conceição, P.R. Wander, S. Dasgupta, M. Das, Int. J. Environ. Stud. **77**(3), 492–509 (2020). https://doi.org/10.1080/00207233.2019.1675295
34. S. Kumari, R. Naraian, J. Environ. Manage. **180**, 172–179 (2016). https://doi.org/10.1016/j.jenvman.2016.04.060
35. U. Lucia, G. Grisolia, A.L. Kuzemsky, Entropy **22**(8), 887–898 (2020). https://doi.org/10.3390/e22080887
36. G. Grisolia, D. Fino, U. Lucia, Energy Rep. **6**, 1561–1571 (2020). https://doi.org/10.1016/j.egyr.2020.06.014
37. N.R. Caetano, R. Cataluña, H.A. Vielmo, Int. Review Mech. Eng. **9**(2), 124–128 (2015). https://doi.org/10.15866/ireme.v9i2.4341
38. N.R. Caetano, D. Soares, R.P. Nunes, F.M. Pereira, P.S. Schneider, H.A. Vielmo, F.T. van der Laan, Open Eng. **5**, 213–219 (2015). https://doi.org/10.1515/eng-2015-0016
39. N.R. Caetano, G. Lorenzini, A.R. Lhamby, V.M.M. Guillet, M.A. Klunk, L.A.O. Rocha, Int. J. Heat Technol. **38**, 1–8 (2020). https://doi.org/10.18280/ijht.380101
40. N.R. Caetano, T.Z. Stapasolla, F.B. Peng, P.S. Schneider, F.M. Pereira, H.A. Vielmo, Defect Diffus. Forum **362**, 29–37 (2015). https://doi.org/10.4028/www.scientific.net/DDF.362.29
41. N.R. Caetano, M.S. Venturini, F.R. Centeno, C.K. Lemmertz, K.G. Kyprianidis, Therm. Sci. Eng. Prog. **7**, 241–247 (2018). https://doi.org/10.1016/j.tsep.2018.06.008
42. M. Khatamian, M. Irani, J. Iran. Chem. Soc. **6**, 187–194 (2009). https://doi.org/10.1007/BF03246519
43. M.A. Klunk, S. Dasgupta, M. Das, M.G. Cunha, P.R. Wander, E.C.S.J. Solid, State Sci. Technol. **8**(10), N144–N150 (2019). https://doi.org/10.1149/2.0131910jss
44. M.A. Klunk, S. Dasgupta, M. Das, P.R. Wander, Z. Shah, Per. Tchê Quím. **16**(33), 70–81 (2019)
45. M.K. de Souza, M.A. Klunk, S.J.S. Xavier, M. Das, S. Dasgupta, Per. Tchê Quím. **17**(35), 816–822 (2020)
46. F. Ma, Q. Jin, P. Li, Z. Chen, J. Lu, Z. Guo, W. Wu, Appl. Geochem. **84**, 325–336 (2017). https://doi.org/10.1016/j.apgeochem.2017.07.002
47. M.A. Klunk, Z. Shah, P.R. Wander, Per. Tchê Quím. **16**(32), 279–286 (2019)
48. M.A. Klunk, M. Das, S. Dasgupta, A.N. Impiombato, N.C. Caetano, P.R. Wander, C.A.M. Moraes, Mater. Res. Express **7**, 015023 (2020). https://doi.org/10.1088/2053-1591/ab608d
49. M.A. Klunk, S.B. Schröpfer, S. Dasgupta, M. Das, N.R. Caetano, A.N. Impiombato, P.R. Wander, C.A.M. Moraes, Chem. Pap. **74**, 2481–2489 (2020). https://doi.org/10.1007/s11696-020-01095-4
50. M. Das, S. Dasgupta, M.A. Klunk, S.J.S. Xavier, F. ChemaleJunior, P.R. Wander, Can. J. Chem. **98**(10), 609–615 (2020). https://doi.org/10.1139/cjc-2020-0142
51. M.A. Klunk, S. Dasgupta, B.V.G. Nunes, P.R. Wander, Per. Tchê Quím. **16**(31), 778–783 (2019)
52. M. Wdowin, M. Franus, R. Panek, L. Badura, W. Franus, Clean Technol. Environ. **16**(6), 1217–1223 (2014). https://doi.org/10.1007/s10098-014-0719-6
53. V. Somerset, Talanta **64**(1), 109–114 (2004). https://doi.org/10.1016/j.talanta.2003.10.059
54. K. Elaiopoulos, T. Perraki, E. Grigoropoulou, Microporous Mesoporous Mater. **134**(1–3), 29–43 (2010). https://doi.org/10.1016/j.micromeso.2010.05.004
55. J.T. Kloprogge, *Infrared and Raman Spectroscopies of Clay Minerals* (Elsevier, Amsterdam, 2017), pp. 150–199. https://doi.org/10.1016/b978-0-08-100355-8.00006-0
56. T.G. Ryu, G.J.C. Ryu, C.H. Choi, C.G. Kim, S.J. Yoo, H.S. Yang, Y.H. Kim, J. Ind. Eng. Chem. **12**, 401–407 (2006)
57. R. Nitzsche, A. Gröngröft, M. Kraume, Sep. Purif. Technol. **209**, 491–502 (2019). https://doi.org/10.1016/j.seppur.2018.07.077
58. V.K. Singh, E.A. Kumara, Mater. Today Proc. **5**(11), 23033–23042 (2018). https://doi.org/10.1016/j.matpr.2018.11.032
59. Q. Chen, R. Zhu, H. Fu, L. Ma, J. Zhu, H. He, Y. Deng, Microporous Mesoporous Mater. **260**, 76–83 (2018). https://doi.org/10.1016/j.micromeso.2017.10.033